Journal of Power Sources 191 (2009) 280–288

Contents lists available at ScienceDirect

Journal of Power Sources

journal homepage: www.elsevier.com/locate/jpowsour

Promotional effect of upper Ru oxides as methanol tolerant electrocatalyst for the oxygen reduction reaction

M. Montiel [a], P. Hernández-Fernández [a], J.L.G. Fierro [b], S. Rojas [b,*], P. Ocón [a,**]

[a] Departamento de Química-Física Aplicada C-II, Campus UAM, 28049 Madrid, Spain
[b] Instituto de Catálisis y Petroleoquímica (CSIC), C/Marie Curie 2, 28049 Madrid, Spain

ARTICLE INFO

Article history:
Received 5 December 2008
Received in revised form 5 February 2009
Accepted 7 February 2009
Available online 20 February 2009

Keywords:
PtCoRu nanoparticles
Ruthenium oxide
Oxygen reduction reaction
Methanol tolerance
Methanol crossover
XPS

ABSTRACT

The role of Ru on the oxygen reduction reaction in the presence of methanol has been investigated. To this end a series of carbon supported Pt based electrocatalysts containing Ru and Co have been prepared and thoroughly characterized. The catalytic performance on the oxygen reduction reaction (ORR) both in the presence and in the absence of methanol by linear sweep voltammetry on rotating disk electrode has been studied. In spite of its documented ability towards methanol and CO oxidation, when Ru-containing catalysts are subjected to excursions to potentials more positive than 0.8 V vs. NHE they develop a certain tolerance to the presence of methanol. This feature is attributed to the formation of upper oxide Ru species that impede the methanol oxidation reaction to occur under the typical reaction conditions of the oxygen reduction process, i.e. potentials more positive than 0.7 V vs. NHE and oxygen saturated atmospheres. The evolution of Ru species with the applied potential has been investigated by XPS, identifying the presence of upper oxidized Ru phases.

1. Introduction

The development of direct methanol fuel cells (DMFCs) has been an objective of several research groups for more than 30 years [1,2]. The performance of DMCFs is limited by various drawbacks, including kinetics constraints, catalyst poisoning and methanol crossover from the anode to the cathode side through the membrane [3,4]. An obvious approach to reduce the methanol crossover effect consists in the development of non-permeable membranes [5]. From the catalytically point of view, the attention is paid to the development of catalyst that do not adsorb methanol under the typical operation conditions during the oxygen reduction reaction (ORR) [6]. This latter approach should be conducted in parallel to the developing of catalysts displaying superior performance on the ORR itself. Generally both approaches imply the preparation of bi- or even tri-metallic catalysts [7].

Economic considerations apart, platinum alloys such as PtCo and PtNi are the best catalysts for the ORR and they are thus far the only realistic option as cathode electrode in low temperature fuel cells [8,9]. Pt provides the lowest overpotential and the highest selectivity towards the direct oxygen reduction to water, yielding only a small amount of hydrogen peroxide [10–13]. However, at potentials more positive than 0.7 V vs. NHE, Pt is covered by and oxide layer, which impedes the adsorption of O_2.

The oxygen reduction reaction depends on the nature of the Pt surface (allowed or not, oxidized or reduced, etc.). In order to reduce the amount of Pt required for fuel cell applications, a range of Pt binary alloys exhibiting good activity for the ORR has been reported [14–18]. The approach consisted in alloying Pt with other transition metals that increases the value of Pt d-band vacancies per atom in order to increase the ORR [19]. Also, alloying Pt with atoms that modify the oxophylicity of the particles seems to improve the kinetics on the ORR by impeding the formation of the oxide layer that competes with O_2 adsorption [20].

On the other hand, the unique electrocatalytic activity of Pt becomes severely suppressed by the presence of CO in the feed. It is well established that alloying Pt with metals such as Mo, Sn or Ru results in electrocatalysts with improved tolerance to CO poisoning [21,22]. Two approaches have been evoked the beneficial effect of Ru: (i) nucleation of Ru–OH_{ad} species at potentials more positive than Pt–OH_{ad} ones and (ii) electronic modification of Pt, thus weakening the Pt–CO bond. The former one, the so-called bifunctional effect is the preferred explanation [23], although a certain contribution from the latter one, the ligand effect, cannot be ruled out [24]. The actual nature of the Ru phase in the bimetallic catalysts is elusive. Whereas early studies pinpointed bimetallic alloyed phases as the active sites, many studies claim enhanced methanol electrooxidation due to the presence of Ru oxides, or more likely hydrous ruthenium oxides [25–27]. Irrespectively of

* Corresponding author. Fax: +34 91 497 4785.
** Corresponding author.
E-mail addresses: srojas@icp.csic.es (S. Rojas), pilar.ocon@uam.es (P. Ocón).

0378-7753/$ – see front matter © 2009 Elsevier B.V. All rights reserved.
doi:10.1016/j.jpowsour.2009.02.023

the actual nature of the active phase, the promotional effect of Ru in the methanol or CO electrooxidation is observed at potentials less positive than 500 mV; at more positive potentials, Pt based electrocatalysts display higher oxidation current densities than PtRu ones [28,29]. Published works in the field of DMFC usually do not show cyclic voltammetry studies of the methanol oxidation on PtRu. In fact, those studies are not usually conducted at potentials more positive than 800 mV, nor do they show the reverse scan of the process. However, if methanol oxidation is studied by cyclic voltammetry reaching potentials more positive than 800 mV [30–32] a peculiar effect can be observed. Methanol oxidation (or more likely, the oxidation of the intermediate species generated during methanol oxidation) seems to be suppressed during the reverse scan. On the contrary, this feature is not observed over bare Pt electrocatalyts.

In this paper, the synthesis of carbon supported PtCoRu nanoparticles by means of the polyol method, their characterization and their performance on the ORR in the presence and in the absence of methanol is reported. X-ray diffraction (XRD), X-ray photoelectron spectroscopy (XPS), and transmission electron microscopy (TEM) are used for characterization of the catalysts. The study of the ORR on PtCoRu/C and PtCo/C electrodes in sulfuric acid solutions in presence of methanol by means of the thin film rotating disk electrode technique was undertaken. The influence of the presence of 0.1 M methanol within the ORR medium was evaluated. Commercial catalysts Pt/C 40 wt%, and PtRu/C 30 wt% (Johnson–Matthey, atomic ratio 1:1, particle size 2.5 nm) were selected as reference materials.

2. Experimental

2.1. Catalysts preparation

The synthesis of PtCo and PtCoRu nanoparticles was carried out by using the polyol technique [33,34]. This method consists on the stabilization and subsequent reduction of the desired metallic precursor in a liquid alcoholic medium (ethylene glycol, glycerol, etc.) at moderate temperatures. The alcohol acts as both the reducing agent and dissolving medium. This method allows a precise control of the size and the shape of the metal particles by means of the amount of water added during the synthetic process, since it determines the final size of the colloid where the metal precursor is located during the reduction process.

Ethylene glycol (EG) was chosen as the synthesis medium and Vulcan XC 72R was used as support of the metallic nanoparticles.

Briefly, an EG solution of each metal precursor, $CoCl_2$, H_2PtCl_6 and $RuCl_3$, was added dropwise to a suspension of the support in EG under vigorous stirring. Previously, the suspension containing the carbon was stirred and treated in an ultrasonic bath for 30 min. The mixture was stirred for 4 h. Afterwards, a 2.5 M in EG solution of NaOH to adjust the pH around 13 was added. The total amount of water was 5 vol.%. Then, the solution was refluxed at 140 °C for 3 h to ensure the total reduction of the metallic precursors. In order to remove the organic intermediates of the reaction (glyoxal, oxalic acid, glycolic acid, etc.) the process was carried out under flowing N_2. The solid obtained was thoroughly rinsed with water and dried at 70 °C for 8 h. The synthesized electrocatalysts are labelled as PtCo/C and PtCoRu/C.

2.2. Physical characterization

X-ray diffraction patterns were collected on a Seifert 3000 powder diffractometer, operating with Cu Kα radiation (λ = 0.15418 nm) generated at 40 kV and 40 mA. Scans at 0.02° s^{-1} for 2θ values between 10° and 90° were recorded. The display and handling of the diffraction patterns as well as unit cell refinements were carried out using the PowderCel software [35].

X-ray photoelectron spectra (XPS) of the samples were acquired with a VG Escalab 200R spectrometer fitted with a Mg Kα ($h\nu$ = 1253.6 eV) 120 W X-ray source. Samples were pressed into small stainless-steel cylinders and mounted on a sample rod, placed in a pretreatment chamber, and degassed at room temperature and 10^{-5} mbar for 5 h prior to transfer to the analysis chamber. Residual pressure was maintained below 3×10^{-8} mbar. The 50 eV energy regions of the photoelectrons of interest were scanned a number of times to obtain an acceptable signal-to-noise ratio. Intensities were estimated by calculating the integral of each peak, determined by subtraction of the Shirley type background and fitting of the experimental curve to a combination of Lorentzian and Gaussian lines of variable proportions. Accurate binding energies (±0.2 eV) were determined by referencing to the C 1s peak at 284.6 eV. For the study of the effect of the applied potential an isopropanol dispersion of PtCoRu/C was deposited onto a 12.7 mm diameter carbon planchet for electron microscopy applications (Electron Microscopy Sciences). The sample was dried and used as the working electrode in an electrochemical cell as described below. Potential was set at the desired value of 0.8 or 1.2 V for 60 s. The electrode was removed and immediately placed into the analysis chamber of the XPS device. To avoid oxidation from air exposure the electrode was covered with isooctane. During the experiments conducted at 1.2 V oxygen evolution was so vigorous that the PtCoRu/C sample was detached from the graphite electrode. To overcome this issue, a nafion film covering the electrode was applied before the electrochemical experiments. In this manner no catalyst leaching was observed. The Ru 3p core level of a reference sample, tetra-*n*-propylammonium perruthenate(VII), 98% purchased from Alfa Aesar, was also recorded.

The X-ray fluorescence analysis (TXRF) was performed on a Seifert EXTRA-II spectrometer equipped with two X-ray fine focus lines, Mo and W anodes, and a Si(Li) detector with an active area of 80 mm^2 and a resolution of 157 eV at 5.9 keV (Mn Kα).

Specimens for TEM analyses were prepared by dispersing the powder samples in isobutanol. One drop of the resulting suspension was placed on a holey carbon film supported by a copper grid. They were studied on a JEM 2100F device equipped with an EDAX detector for X-ray energy dispersive spectroscopy analysis.

2.3. Electrochemical characterization

The synthesized samples, PtCo/C and PtCoRu/C, were tested as electrocatalysts for the oxygen reduction reaction. Their performance was compared to that of commercial (Johnson–Matthey) 40 wt% Pt/C and 30 wt% PtRu/C catalysts.

Rotating disk electrode (RDE) studies were carried out at 25 °C in a conventional three-compartment electrochemical glass cell. A glassy carbon rotating disk electrode (0.071 cm^2, GC-Typ zu628) was used as a substrate for the catalyst. Previous to each test, the electrode was polished with alumina 0.05 μm to obtain a mirror finish, and it was rinsed with triply distilled water in an ultrasonic bath. A mercury/mercurous sulphate K_2SO_4 saturated electrode and a gold plate as the reference and the counter electrodes were used. In the manuscript, all potentials are referred to the normal hydrogen electrode (NHE).

The samples under study were deposited onto the working electrode by means of an ink. Typically, 5 mg of the electrocatalyst, 30 μL of 5 wt% of Nafion solution (Aldrich), and 700 μL of Milli-Q water were dispersed in an ultrasonic bath for 45 min, obtaining a homogenous ink. Five microliters of the ink were dropped onto the electrode and dried at room temperature for 15 min resulting in a homogenous coating. This leads to a final Pt loading of 10.3 μg for the PtCo/C, 9.6 μg for PtCoRu/C and 13.7 and 6.8 μg for Pt/C and PtRu/C, respectively. A 0.5 M H_2SO_4 (Merck) was used as the electrolyte. All solutions were prepared with Milli-Q water.

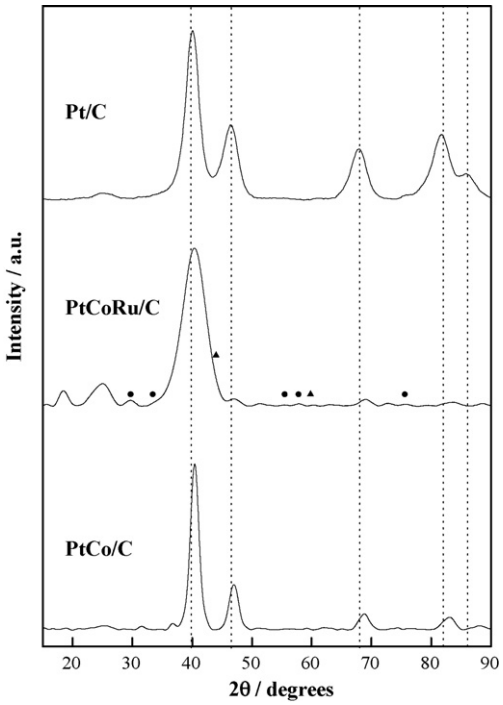

Fig. 1. XRD diffractograms of Pt/C, PtCoRu/C and PtCo/C samples: (●) RuO_2 and (▲) Co_3O_4.

Electrochemical measurements were performed with a potentiostat/galvanostat EG&G 273A controlled by computer. The electrode rotation speed was regulated by a Metrohm 628-10 unit. The rotation rate was varied from 500 to 2500 rpm.

In order to clean and activate the electrode surface and to study the methanol electrooxidation process, a series of cyclic voltammetry (CV) experiments were done. Prior to each CV measurement the electrolyte was purged with nitrogen (air liquid) for 30 min to deareate the system. The samples were cycled at 100 mV s^{-1} between 0.0 and 0.8 V until reproducible voltammograms were obtained. Then, methanol electrooxidation was studied by CV from N_2 saturated 0.1 M CH_3OH/0.5 M H_2SO_4 solutions recorded at 10 mV s^{-1}.

Linear sweep voltammetry for the study of the oxygen reduction reaction both in the presence and in the absence of methanol was used. The electrolyte was saturated with high purity oxygen (air liquid) for 20 min. The polarization curves were obtained at different rotation rates between 1.1 and 0.05 V at room temperature.

3. Results and discussion

Fig. 1 depicts the diffractograms of the PtCo/C, PtCoRu/C and Pt/C electrocatalysts. In all samples, reflections from the carbon support and the Pt fcc structure are observed. The presence of Co_3O_4 (JPDS#78-1970) and RuO_2 (JPDS#73-1469) was detected in PtCoRu/C. The reflections corresponding to the Pt fcc crystalline structure of PtCo/C and PtCoRu/C are shifted to higher 2θ values compared to those of Pt/C. In agreement with Vegard law, this shifting would correspond to a contraction of the Pt lattice. The lattice parameters of PtCo/C and PtCoRu/C, respectively, 3.8498 and 3.8356 Å, are smaller than that of Pt/C, according to the contraction of the lattice due to the incorporation of Co and Ru. Pt exhibits an fcc structure, whereas Co and Ru exhibit a hexagonal close-packed (hcp) ones. Therefore it is difficult to assess the actual degree of alloying from the lattice constant values of the solids [36]. The particle size calculated by applying the Scherrer equation to the 200 reflections is ca. 5.5 nm. This value is in good agreement with the average particle size deduced from the observation of the TEM images. For the construction of the histograms more than 200 particles were considered. Selected micrographs representative of the particles and the corresponding histograms are depicted in Fig. 2. Cell parameters, particle size and actual metal content of each catalyst are summarized in Table 1.

Table 1
Structural parameters of the electrocatalysts.

Sample	Particle size[a] (nm)	Cell parameter (Å)	Metallic content[b]		
			Pt (%)	Co (%)	Ru (%)
PtCoRu/C	5.5	3.8356 ± 0.0435	28	5	3
PtCo/C	5.5	3.8498 ± 0.0220	30	10	
Pt/C	3.5	3.9075 ± 0.0026	40[c]		

[a] Particle size calculated from the Scherrer equation. The 2 2 0 reflection was selected in order to overcome the contribution of the graphite phase.
[b] Pt, Co and Ru content determined from TXRF analysis.
[c] Pt content provided by the supplier (Johnson–Matthey).

XPS spectra of Pt 4f, Ru 3p and 3d, O 1s, C 1s and Co 2p core levels of the samples were analyzed. The binding energy and relative abundance of surface species, both for PtCoRu/C and PtCo/C are summarized in Tables 2A and 2B. The core level energy region of the samples consists of three doublets whose most intense Pt $4f_{7/2}$ peaks appear at binding energies of ca. 71.6, 73.2 and 74.9 eV (actual values for each sample are collected in Table 2A) ascribed to Pt^0, PtO and PtO_2, respectively [37]. As deduced from data depicted in Table 2B, the relative abundance of the Pt species is higher in sample PtCoRu/C than in sample PtCo/C. The most intense Co $2p_{3/2}$ peak of the Co 2p core level region displayed two components at binding energies of ca. 780 and 782 eV corresponding to CoO and Co_3O_4 species, respectively. The relative abundance of each species is collected in Table 2B.

Since the binding energy of the most intense Ru 3d core level overlaps with that of the C 1s, the Ru 3p region was analyzed [38]. The Ru $3p_{3/2}$ spectrum contains a single broad component that can be attributed to RuO_2 or $RuO_2{\cdot}xH_2O$ species [26,39,40].

Fig. 3 shows the cyclic voltammograms of PtCo/C and PtCoRu/C in H_2SO_4 solution at 50 mV s^{-1}. For the sake of comparison, the voltammograms of Pt/C and PtRu/C recorded under identical conditions are also depicted. On the Pt/C sample, the hydrogen adsorption/desorption features between 0 and 0.3 V, followed for the double layer potential region are visible. The hydrogen adsorption/desorption features over PtCo/C are also clearly observed. However, for the Ru-containing samples, the hydrogen adsorption/desorption become ill resolved. On Pt/C, the oxide formation

Table 2A
Binding energies (eV) of core electrons of PtCoRu/C, PtCo/C and Pt/C samples referred to C 1s at 284.6 eV.

Catalyst	O 1s	Pt $4f_{7/2}$	Ru $3p_{3/2}$	Co $2p_{3/2}$
PtCoRu/C	530.1 (50)	71.6 (70)	462.4	780.3 (71)
	531.3 (34)	73.2 (17)		782.6 (29)
	532.5(16)	74.9 (13)		
PtCo/C	530.2 (30)	71.4 (66)		779.5 (28)
	531.5 (42)	72.8 (24)		781.3 (72)
	532.6 (27)	74.5 (11)		
Pt/C	530.3 (44)	71.5 (55)		
	531.5 (35)	73.1 (25)		
	532.6 (21)	74.9 (20)		

Table 2B
Atomic ratio determined from the XPS data.

Catalyst	Pt/C	Co/C	Ru/C	Pt/Ru	Pt/Co
PtCoRu/C	0.053	0.010	0.012	4.6	5.5
PtCo/C	0.015	0.049	–	–	1.3

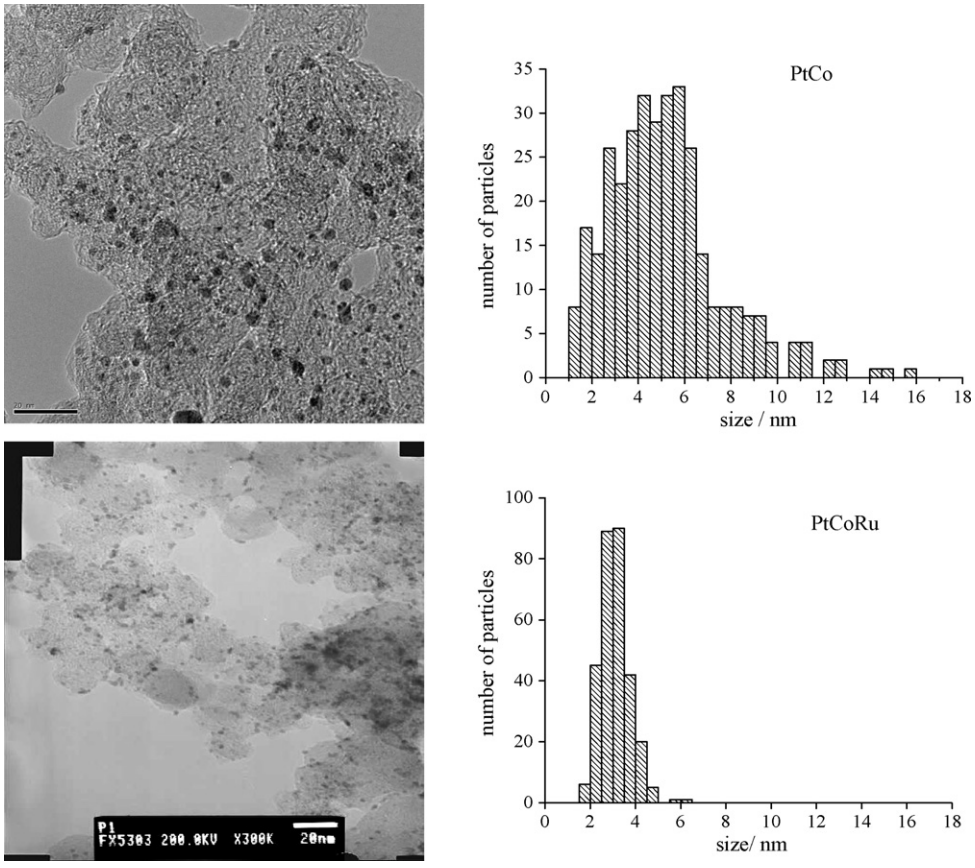

Fig. 2. Representative TEM micrographs of PtCo/C and PtCoRu/C samples.

commences at ca. 0.75 V, being shifted to more positive potentials on the PtCo/C sample. On the contrary, the onset of the formation of oxides over the Ru-containing samples is shifted to less positive potentials. As depicted in Fig. 3, between 0.3 and 0.7 V the profile of Pt electrodes display a constant current value, however, the profile of the voltammograms for the Ru samples within the same potential region depicts a constant increase in the current response due to the formation Ru oxides. This feature coincides with already published results [41]. In fact the more facile nucleation of OH species over Ru at potentials lower than 0.4 V is considered as the responsible of the enhancement of the CO tolerance displayed by PtRu bimetallic samples, the so called bifunctional effect [42,43]. In spite of the relatively low content of Ru on PtCoRu/C, its effect is evident commencing the oxide formation region at potentials ca. 0.6 V. The position of the oxide reduction peak on the reverse sweep of all samples is also very informative. Oxide reduction is more irreversible on the Ru-containing samples (the peak position is shifted to less positive potentials). On the contrary, PtCo/C facilitates the process, the peak potential (Ep) of the oxidation process on PtCo/C being located at the most positive potentials of the series. Clearly two antagonist effects coexist, whereas Ru promotes oxide formation, the presence of Co impedes it, shifting the potential to more positive values with respect to that of the Pt/C. This latter effect is also well documented and it accounts to the oxophylicity of the samples [8,18,44]. It must be stressed that the presence of Ru not only favours the formation of oxides, it also difficult their reduction during the reverse scan. To the best of our knowledge, this feature has not been discussed in literature. This lack of discussion is not surprising since the role of Ru is the promotion of CO and methanol oxidation reactions at potentials as less positive as possible, so the chemical state of Ru on the reverse scan is neglected. However, this feature could turn out to be of a great importance for the designing of methanol tolerant cathode electrocatalysts as it will be discussed below. Before that, the oxygen reduction reaction over the prepared catalysts will be detailed.

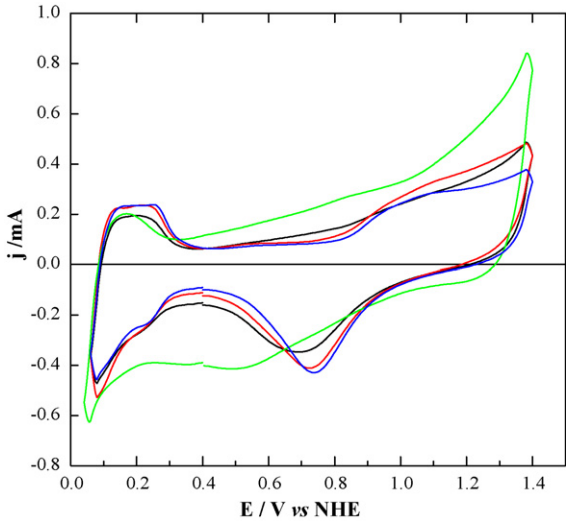

Fig. 3. Cyclic voltammograms on PtCoRu/C (black), PtCo/C (blue), PtRu/C (green) and Pt/C (red) electrodes obtained in N_2 saturated 0.5 M H_2SO_4 solution at 50 mV s^{-1}. (For interpretation of the references to colour in this figure legend, the reader is referred to the web version of the article.)

The kinetic of the ORR on PtCo/C and PtCoRu/C, and the reference samples, in oxygen saturated 0.5 M H_2SO_4 media by using a rotating disk electrode (RDE) and using the thin film method [45] was studied. Oxygen saturation was achieved by bubbling oxygen for

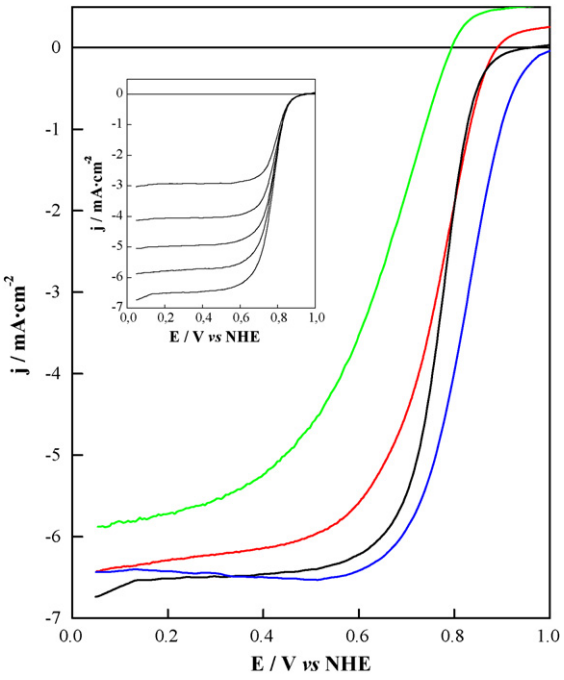

Fig. 4. Current density profile during the ORR on PtCoRu/C (black), PtCo/C (blue), PtRu/C (green) and Pt/C (red) obtained in oxygen saturated 0.5 M H_2SO_4 solution at 2500 rpm and 1 mV s^{-1}. (Inset) Current density profile obtained during the ORR on PtCoRu/C recorded at 1 mV s^{-1} on oxygen saturated 0.5 M H_2SO_4 at different rotation rates, 500, 1000, 1500, 2000 and 2500 rpm. (For interpretation of the references to colour in this figure legend, the reader is referred to the web version of the article.)

20 min and it was maintained during the experiment. Fig. 4 depicts the performance of PtCoRu/C, PtCo/C, PtRu/C and Pt/C on the ORR recorded at 2500 rpm under the same experimental conditions. Both PtCoRu/C and Pt/C samples display a similar performance on the ORR reaction. Nevertheless, the performance of PtCo/C is the best of the series, displaying lower overpotentials in the kinetic and mixed controlled regions than PtCoRu/C and Pt/C. Also, the onset of the ORR on PtCo/C is found at the most positive potential value of the series. The positive effect of Co on the ORR accounts to the increasing amount of Pt sites for the adsorption of O_2 [18]. For the sake of comparison, the performance of a commercial PtRu/C catalyst is also depicted in Fig. 4. It can be observed that its performance on the ORR is rather poor. In fact, PtRu/C formulation is adequate for the anodic oxidation of alcohols rather than for the reduction of O_2. The inset to the figure depicts the polarization curves recorded during the oxygen reduction on PtCoRu/C at selected rotation rates from 500 to 2500 rpm. All samples display a similar pattern as a function of the rotation rate. Three different regions can be distinguished for each rotation rate: the diffusion-limited region, between 0.0 and 0.5 V; the mixed control region, from 0.5 to 0.8 V; the kinetic control region, from 0.8 V. In order to evaluate the performance of the catalyst during the reaction the Koutecky–Levich equation was used:

$$\frac{1}{j} = \frac{1}{j_k} + \frac{1}{j_d} \tag{1}$$

According to this equation, the total measured current density (j) during ORR is related to the kinetic current density (j_k), owing to charge transfer, and to the diffusion-limiting current (j_d), owing to the mass transport.

According to the Levich equation, j_d can be expressed as:

$$j_d = 0.62 n_e F D_{O_2}^{2/3} C_{O_2} \nu^{-1/6} \omega^{1/2} = B\omega^{1/2} \tag{2}$$

where j_d is the diffusion-limiting current density, 0.62 is a constant used when ω (rotation rate of the disk electrode) is expressed in radians per second, n_e is the number of electrons transferred per O_2 molecule, F the Faraday constant, D_{O_2} the diffusion coefficient of oxygen in the solution (1.90×10^{-9} cm^2 s^{-1}), C_{O_2} the concentration of oxygen dissolved (1.10×10^{-6} mol cm^{-3}), ν the cinematic viscosity of the sulfuric acid (1.01×10^{-2} cm^{-2} s^{-1}), and B is the Levich constant.

The Koutecky–Levich plots (j^{-1} vs. $\omega^{1/2}$), see Fig. 5, afforded straights lines with a non-zero intercept. A more precise analysis of the data should include deviations due to the presence of internal diffusion phenomena due to the presence of a Nafion layer surrounding the metallic particles, thus covering the active sites. This situation would be analogous to a film-coated electrode surface (Eq. (3)), where j_f is the film diffusion-limiting current density [46]:

$$\frac{1}{j} = \frac{1}{j_k} + \frac{1}{j_f} + \frac{1}{j_d} = a + \frac{1}{B\ \omega^{1/2}} \tag{3}$$

Since the Nafion film is extremely thin, the film resistance is sufficiently small, typically 0.01 cm^2 mA^{-1}, its contribution can be neglected [46].

A first insight into the efficiency of electrocatalysts can be obtained from the value of n_e:

$$O_2 + 2H^+ + 2e^- \rightarrow H_2O_2 \tag{4}$$

$$O_2 + 4H^+ + 4e^- \rightarrow 2H_2O \tag{5}$$

The ORR proceeds either through 2 or 4 electrons mechanism depicted, respectively, in Eqs. (4) and (5). The number of electrons calculated for both PtCo/C and PtCoRu/C is ca. 3.8 indicating a preferential 4-electron pathway reaction on either electrocatalyst.

The kinetic analysis of the catalysts was further completed with the Tafel plots, obtained values are collected in Table 3. In order to determine the kinetic current density properly, the mass transport corrected Tafel plots are obtained. According to the rotating disk electrode theory and assuming that the ORR is a first-order

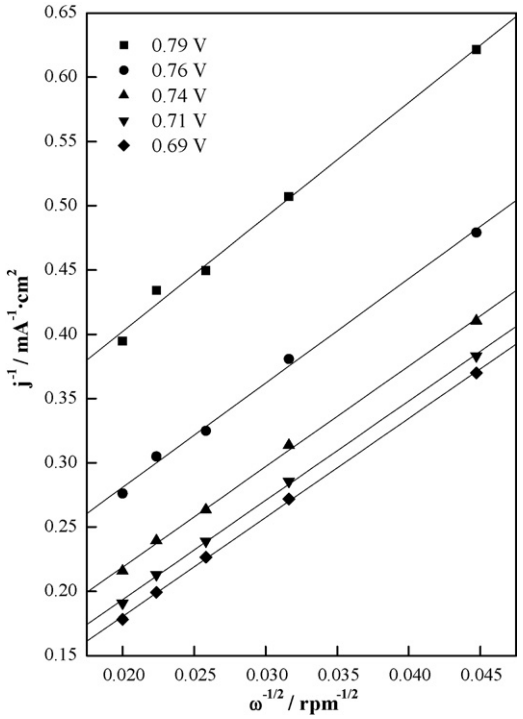

Fig. 5. Levich–Koutecky plots for the ORR on PtCoRu/C at various potentials extracted from the data in the inset of Fig. 4.

Table 3
Kinetic parameters obtained for the electrocatalysts. j_{pf}/j_{pr} values calculated from the MeOH electrooxidation experiments (Fig. 7) after potential excursions to 1.1 and 0.8 V. LO and HO account to low and high overpotential from the ORR, respectively.

Sample	Tafel slope (mV dec^{-1})		j_0 (mA cm^{-2})[a]		j_{pf}/j_{pr}	
	LO	HO	LO	HO	1.1 V	0.8 V
PtCoRu/C	−0.060	−0.120	2.322E−08	2.591E−04	0.7	0.9
PtCo/C	−0.063	−0.117	8.054E−06	2.132E−03	0.9	1.0
Pt/C	−0.060	−0.120	3.746E−08	2.752E−04	1.2	1.0
PtRu/C	−0.062	−0.123	2.658E−09	4.846E−05	0.3	0.6

[a] j_0 calculated for geometric surface area.

reaction the kinetic current in the mixed activation-diffusion region is calculated from the following equation [47]:

$$j_k = \frac{j_d j}{j_d - j} \tag{6}$$

where j_k is the kinetic current density, j is the measured current density during the oxygen reduction polarization and j_d is the diffusion limiting current density, given by Eq. (2).

The relationship between the kinetic current density and the overpotential can be expressed as a Tafel form:

$$\eta = \frac{2.3RT}{\alpha nF}\log(j_0) - \frac{2.3RT}{\alpha nF}\log(j_k) \tag{7}$$

where η is the overpotential, R is the gas constant, T is the temperature, F is the Faraday constant, n is the electron transfer

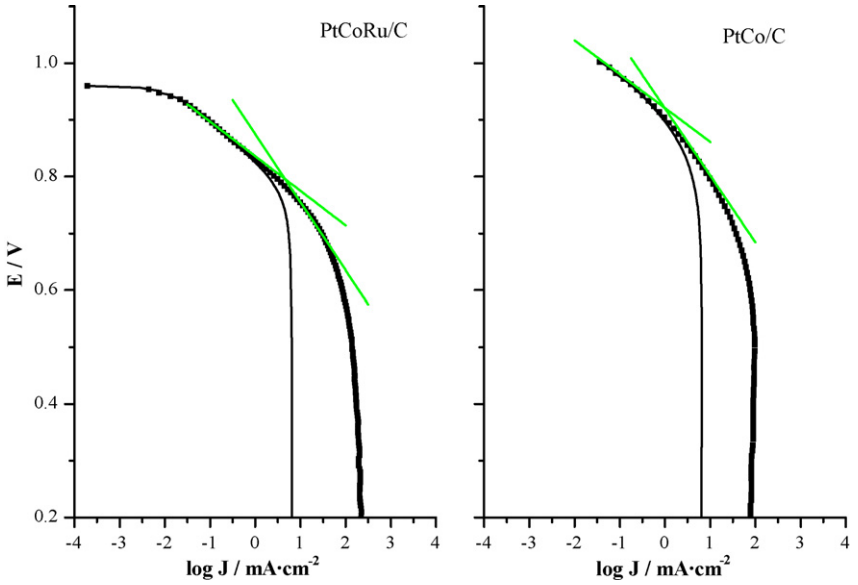

Fig. 6. Corrected Tafel plot of the samples PtCo/C and PtCoRu/C.

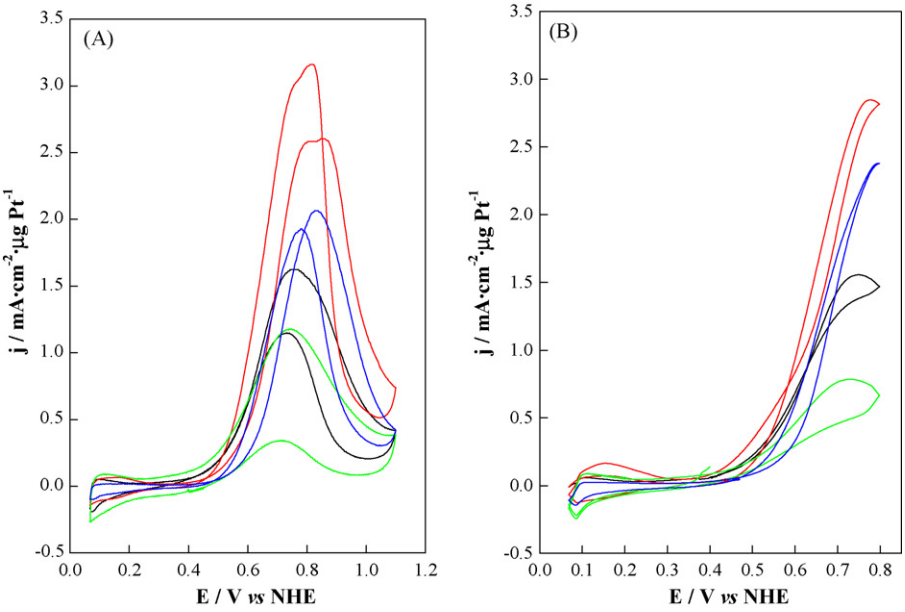

Fig. 7. Methanol oxidation profile on PtCoRu/C (black), PtCo/C (blue), PtRu/C (green) and Pt/C (red) electrodes recorded in N_2 saturated 0.1 M CH_3OH/0.5 M H_2SO_4 at 10 mV s^{-1}. Scans were recorded from: (A) 0.05–1.1 V and (B) 0.05–0.8 V. (For interpretation of the references to colour in this figure legend, the reader is referred to the web version of the article.)

number in the rate-determining step of the ORR, α is the electron transfer coefficient and j_0 is the value of the exchange current densities.

The j_0 (current exchange density) values obtained from the intercept of the mass transfer corrected Tafel plots (Fig. 6) are shown in Table 3. Both PtCoRu/C and Pt/C display similar values which are in line with values already reported for analogous systems [48].

In summary, PtCo/C is the best catalysts for the ORR. The performance of the trimetallic catalyst on the ORR is rather similar to that of the commercial sample (Pt/C) in spite of the lower amount of Pt of the former. The performance of a commercial PtRu/C sample in the ORR is worst than that of the other samples. Thus far it seems reasonable to assume that Ru either has no effect on the ORR other than acting as a diluting species or it actually impedes the reaction by acting as a poison species. On the contrary, the presence of Co seems to favour the ORR. It must be recalled at this point that the actual amount of Ru on the trimetallic sample is ca. 3 wt%.

However, as stated in Section 1, the aim of our research was to investigate catalysts' tolerance to methanol during the oxygen reduction reaction. As discussed in previous sections, Ru is added to Pt based electrocatalysts to promote CO oxidation at less positive potentials than Pt alone. Also, we have observed (Fig. 3) that after excursions to potentials more positive than 1.0 V, the presence of Ru favours the formation of more irreversible oxide-layers. In fact, there are several publications that reveal how, contrary to the process over Pt/C, the methanol oxidation reaction over PtRu/C shows very low oxidation currents on the reverse sweep [30–32].

With these considerations in mind, the ORR in O_2 saturated 0.1 M CH_3OH/0.5 M H_2SO_4 electrolyte was studied. First the methanol oxidation reaction in oxygen free atmosphere was studied by cyclic voltammetry. Fig. 7 depicts the cyclic voltammograms recorded at 10 mV s^{-1} and 25 °C. It can be observed that for the Ru-containing electrodes the onset of the methanol oxidation process in the forward scans is shifted to less positive potentials. Noticeably, the extension of the methanol oxidation process on the Ru-containing samples is the lowest of the series and it appears to be related to the actual Ru content on the electrodes. The onset of the oxidation process is shifted to less positive potentials and the j_{pf}/j_{pr} ratio is the lowest of the series. The j_{pf}/j_{pr} (j_{pf}: forward peak current density; j_{pr}: reverse peak current density) ratio can be taken as a measure of the catalytic performance; the higher the value, the better the methanol electrooxidation is [49]. For the Ru-containing samples the value depends strongly on the window potential studied. Thus if the potential excursions to positive values is stopped at 1.1 V (Fig. 7A), the j_{pf}/j_{pr} ratio value is rather low, however, it increases by twofold when potential excursions were stopped at 0.8 V (Fig. 7B). The j_{pf}/j_{pr} ratio values for all samples are collected in Table 3. The most remarkable issue is the fact that the presence of Ru seems to impede the oxidation of methanol at potentials where the ORR usually takes place.

In order to corroborate this hypothesis, the tolerance of PtCoRu/C to the presence of methanol during the ORR was investigated and compared to that of Pt/C, PtRu/C and PtCo/C. Fig. 8 shows the response obtained from linear sweep voltammetry experiments on the different electrodes. In the absence of methanol, the PtCo/C electrode is the best of the series and the trimetallic electrode also shows a significant performance on the ORR, similar to that of Pt/C, see Fig. 4. If methanol is added to the reaction medium, the picture changes dramatically. The performance of Pt/C and PtCo/C on the ORR is affected severely. In fact the predominant process on those electrodes is the methanol oxidation reaction (MOR) as deduced from the net positive current observed at potentials more positive than 0.58 V. On the other hand, the performance of PtRu/C and PtCoRu/C electrodes on the ORR is only slightly modified by the presence of methanol. Under these reaction conditions, both methanol oxidation and oxygen reduction reactions can take place

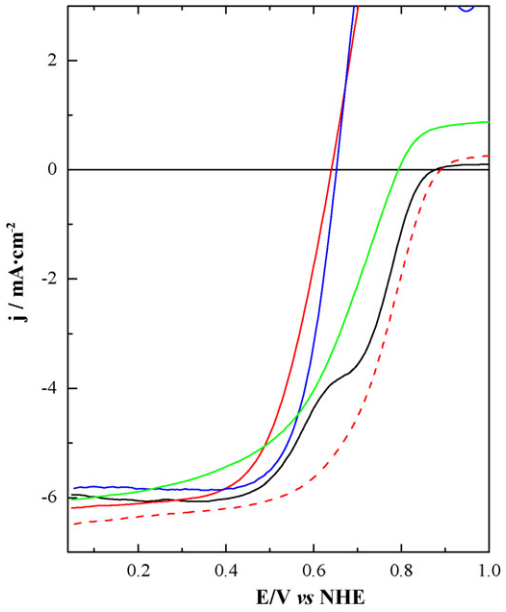

Fig. 8. Current density profile during the ORR in oxygen saturated 0.1 M CH_3OH/0.5 M H_2SO_4 recorded at 10 mV s^{-1}, 2500 rpm on: PtCoRu/C (black), PtCo/C (blue), PtRu/C (green) and Pt/C (red) electrodes. The current density profile of Pt/C recorded in the same experimental conditions obtained from a methanol free is also depicted for comparison (dash red line). (For interpretation of the references to colour in this figure legend, the reader is referred to the web version of the article.)

simultaneously. In principle a fraction of the active sites available for the ORR could be blocked (poisoned) by adsorbed species arising from the methanol oxidation reaction or even by methanol itself. To complicate the picture even more, at potentials more positive than 0.9 V, Pt-oxide formation occurs and both ORR and MOR are hindered.

In the region between 0.40 and 0.85 V, the sign of the net current depended on the chemical nature of the electrodes. As stated above, MOR predominates over Pt/C and PtCo/C electrodes, yielding positive currents, whereas PtRu/C and PtCoRu/C promote the ORR, as evidenced by the negative current, even in the presence of methanol. Clearly, this apparent inhibition of the methanol oxidation reaction displayed by those electrodes can be attributed to the presence of Ru rather than Co, since the PtCo/C sample is strongly affected by the presence of methanol. This result also illustrates how Ru is not removed out of the electrode since otherwise the performance of the electrodes on the ORR should resemble to that of Pt/C or PtCo/C. The performance of Ru is somehow unexpected since Ru is known to promote methanol oxidation on PtRu electrocatalysts. However, as discussed thoroughly in previous sections, the ability towards methanol oxidation on Ru-containing electrodes emerges at potentials less positive than ~0.5 V. If the electrode is exposed to more positive potentials, the methanol oxidation ability is suppressed. During the study of the ORR the electrodes operate at potentials where the Ru oxides are not reduced yet. Therefore, methanol oxidation is not expected to occur over the Ru-containing electrodes. On the contrary, and in good agreement with data depicted in Fig. 6A and B, the magnitude of the methanol electrooxidation over Pt/C and PtCo/C is rather high, almost as good as during the forward scan. Precisely those electrodes display the largest oxidation current during the ORR in the presence of methanol as depicted in Fig. 8. This concept is graphically illustrated in Fig. 9 where the performance of PtCoRu/C on the ORR in the presence of methanol is superimposed to its voltammogram obtained in methanol-free solutions. It can be observed that only at the potential regions where the oxides are reduced, the sample commences to oxidize methanol. This feature reveals the

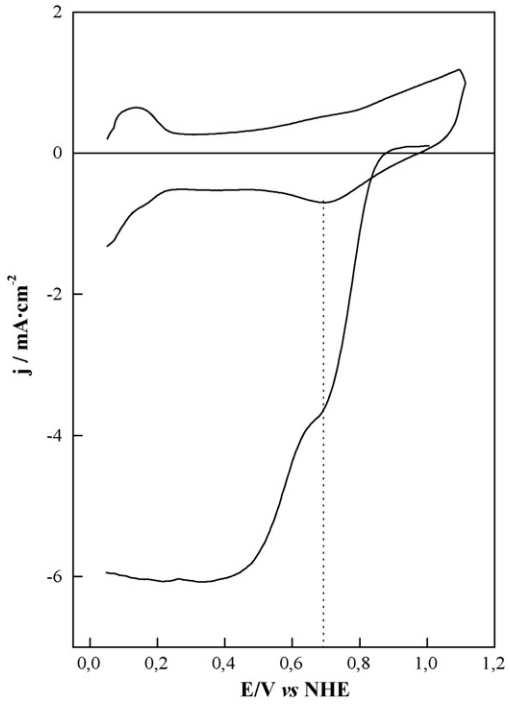

Fig. 9. LSV recorded at 1 mV s^{-1} (in 0.1 M CH_3OH/0.5 M H_2SO_4) and CV recorded at 10 mV s^{-1} (0.5 M H_2SO_4) of sample PtCoRu/C.

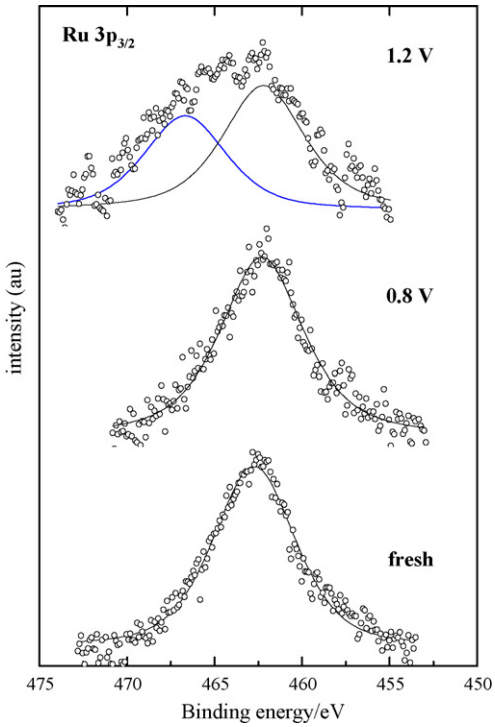

Fig. 10. Evolution of the Ru species detected by XPS analysis of Ru 3p core level of sample PtCoRu/C subjected to 0.8 and 1.2 V. The spectrum of the fresh sample is shown for comparison.

importance of the reversibility of the oxide region for the oxidation of methanol.

Thus far we have hypothesized on how certain Ru oxide species impede methanol electrooxidation. Such species are formed at positive potential (>0.8 V) and are stable under such conditions. In order to confirm the presence of such Ru oxide phases PtCoRu/C samples were deposited onto a graphite disk electrode (as described in Section 2) and analyzed by means of XPS. Then they were subjected to a constant potential program of 0.8 and 1.2 V in 0.5 M H_2SO_4 during 60 s. For the latter program the catalyst was covered with a nafion layer as explained above. Samples were collected, covered with an isooctane layer and rapidly transferred to the XPS analysis chamber. Fig. 10 depicts the Ru $3p_{3/2}$ core level region of the three samples. After excursion to 0.8 V the Ru $3p_{3/2}$ core level region is similar to that of the fresh sample. Remarkably, when subjected to a program potential of 1.2 V, a further Ru component at 466.7 eV appears. The amount of this species is ca. 40 at.% of all Ru on the sample as deduced from XPS data in Table 4. Indeed, there is a lack of data concerning the binding energy of Ru 3p core level in upper valence Ru oxides. Aricò et al. [50] and Raman et al. [51] have ascribed the presence of Ru $3p_{3/2}$ peak at ca. 467 eV (or higher) to $RuO_2{\cdot}xH_2O$. Such assignment was done after Ref. [26], however, this latter reference deals with Ru 3d instead of Ru 3p core levels. Extrapolation of the binding energy of the Ru 3d core level to the Ru 3p core level is not straightforward. Therefore, proper assignments of the high binding energy core level of Ru 3p are necessary. In any case, the high binding energy value found in the spectrum of PtCoRu/C after being subjected to 1.2 V treatment suggest the presence of an upper valence Ru oxide, probably as RuO_4 or RuO_3. The latter species is only stable in the vapour phase at temperatures above 1200 °C [26]. Similarly, RuO_4 has been described as unstable and volatile [49]. However, RuO_4 formation under the reaction conditions similar to those reported in here, i.e. acid media and anodic evolution of O_2 is documented [52–54]. A distinct XPS peak at binding energy of ca. 283 eV is ascribed to the presence of RuO_4 [54]. Alas, the binding energy of the corresponding Ru 3p cope level peaks is not given.

Table 4
Binding energies (eV) of core electrons of PtCoRu/C subjected to different treatments. Peak positions are referred to C 1s at 284.6 eV.

Treatment	Pt $4f_{7/2}$	Ru $3p_{3/2}$
Fresh	71.6 (70) 73.2 (17) 74.9 (13)	462.4
0.8 V	71.4 (49) 72.5 (39) 74.2 (12)	462.5
1.2 V	71.9 (66) 73.5 (23) 75.1 (12)	462.3 (58) 466.7 (42)
Ru(VII)[a]	–	463.6 (70) 466.3 (20)

[a] The XPS spectrum of the Ru 3p core level of tetra-*n*-propylammonium perruthenate(VII) was analyzed as reference.

The Ru 3d core level XPS spectrum of PtCoRu/C was also analyzed (data not shown). However, the Ru 3d signal is overlapped by that of C 1s. A Ru $3d_{5/2}$ contribution at 281.5 eV is observed. The signal is quite broad, suggesting the presence of a peak at ca. 283 eV. However, the presence of the more intense C 1s peaks makes the Ru $3d_{5/2}$ signal difficult to interpret.

Therefore, for a proper assignment of the Ru 3p core level, the binding energy of a commercial perruthenate sample, tetra-*n*-propylammonium perruthenate(VII), has been recorded. The most intense Ru $3p_{3/2}$ peak of the Ru 3p doublet displays two components at 463.6 and 466.3 eV. The former peak can be ascribed to Ru(III) or Ru(IV) species whereas the latter one can be associated to the presence of the expected Ru(VII) ones. As to why the commercial sample displays two contributions it can be speculated about the low stability of upper oxide states either under ambient atmosphere or into the analysis chamber of the XPS [52].

The present study reveals how under ORR reaction conditions, potentials more positive than 1.1 V in the presence of oxygen,

upper oxide Ru species more likely as Ru(VII) or higher are formed. The presence of these upper oxide Ru species impedes methanol electrooxidation, favouring the oxygen reduction reaction. The description of the actual mechanism is out of the scope of this paper, however, since bare Pt or PtCo based catalysts were proved able to oxidize methanol within the potential window where the upper Ru oxides are formed (Fig. 8), the role of Ru on the Pt or PtCo-containing samples must be that of impeding methanol adsorption since otherwise it will be oxidized immediately yielding a net oxidation current instead of the reduction current recorded in the experiment (see Fig. 8).

4. Conclusions

Electrocatalysts based on PtCoRu/C formulations display both a high activity on the ORR and a great tolerance to the presence of methanol. The presence of Ru on carbon supported Pt based electrodes is known to promote CO and methanol oxidation at less positive potentials than bare Pt whereas the presence of Co is beneficial for the ORR. The performance of both Pt and PtCo based catalysts on the ORR is severely affected by the presence of methanol. The poisoning effect of methanol on the ORR can be overcome by adding Ru to the samples provided that upper oxide Ru species are formed. Such Ru species are formed and stabilized under ORR reaction conditions, i.e. potentials more positive than 1.1 V and by the presence of oxygen in the reaction medium.

Acknowledgements

S. Rojas acknowledges to the CSIC-CAM project reference 200680M013 for financial support. P. Ocón acknowledges to CICyT project reference CTQ-2007-66547 for financial support. M. Montiel thanks CAR for a grant.

References

[1] R. Dillon, S. Srinivasan, A.S. Arico, V. Antonucci, J. Power Sources 127 (2004) 112.
[2] G. Apanel, E. Jonson, Cells Bull. 11 (2004) 12.
[3] A.J. Appleby, F.R. Foulkes, Fuell Cell Handbook, Van Remhold, New York, 1989.
[4] S. Gottesfeld, T.A. Zawodzinski, in: R.C. Alkire, H. Gerisher, D.M. Kolb, C.W. Tobias (Eds.), Advances in Electrochemical Science and Engineering, VCH, Weiheim, 1997.
[5] V. Methta, J.S. Cooper, J. Power Sources 114 (2004) 32.
[6] E. Antolini, T. Lopes, E.R. González, J. Alloys Compd. 461 (2008) 253.
[7] P. Hernández-Fernández, S. Rojas, P. Ocón, A. de Frutos, J.M. Figueroa, P. Terreros, M.A. Peña, J.L.G. Fierro, J. Power Sources 177 (2008) 9.
[8] J.X. Wang, N.M. Markovic, R.R. Adzic, J. Phys. Chem. B 108 (2004) 4127.
[9] J.L. Fernández, A.J. Bard, Anal. Chem. 75 (2003) 2967.
[10] M.L. Rao, B.A. Damjanovic, J'.O.M. Bockris, J. Chem. Phys. 67 (1963) 2508.
[11] N.M. Markovic, P.N. Ross, Electrochim. Acta 45 (2000) 4101.
[12] N.M. Markovic, P.N. Ross, Surf. Sci. Rep. 286 (2002) 1.
[13] H.A. Gasteiger, S.S. Kocha, B. Sompalli, F.T. Wagner, Appl. Catal. B 56 (2005) 9.
[14] N. Wakabayashi, M. Takeichi, H. Uchida, M. Watanabe, J. Phys. Chem. B 109 (2005) 5836.
[15] J.R.C. Salgado, E. Antolini, E.R. González, J. Phys. Chem. B 108 (2004) 17767.
[16] H. Yang, W. Vogel, C. Lamy, N. Alonso-Vante, J. Phys. Chem. B 108 (2004) 11024.
[17] L. Xion, A. Manthiram, Electrochim. Acta 50 (2005) 2323.
[18] P. Hernández-Fernández, S. Rojas, P. Ocón, J.L. Gómez de la Fuente, J. San Fabian, J. Sanza, M.A. Peña, F.J. García-García, P. Terreros, J.L.G. Fierro, J. Phys. Chem. C 111 (2007) 2913.
[19] S. Mukerjee, S. Srinivasan, M.P. Soriana, J. McBreen, J. Electrochem. Soc. 142 (1995) 1409.
[20] P. Hernández-Fernández, S. Rojas, P. Ocón, J.L. Gómez de la Fuente, P. Terreros, M.A. Peña, J.L. García-Fierro, Appl. Catal. B: Environ. 77 (2007) 19.
[21] N.M. Markovic, P.N. Ross, CATTECH 4 (2000) 110.
[22] C. Lamy, J.-M. Léger, S. Srinivasan, in: J.O'.M. Bockris, et al. (Eds.), Modern Aspects of Electrochemistry, Number 34, Kluwer Academic/Plenum Publishers, New York, 2001.
[23] H.A. Gasteiger, N. Markovic, P.N. Ross, E.J. Cairns, J. Phys. Chem. 97 (1993) 12020.
[24] P. Liu, J.K. Norskov, Fuel Cells 1 (2001) 192.
[25] J.W. Long, R.M. Stroud, K.E. Swider-Lyons, D.R. Rolison, J. Phys. Chem. B 140 (2000) 9772.
[26] D.R. Rolison, P.L. Hagans, K.E. Swider, J.W. Long, Langmuir 15 (1999) 774.
[27] S. Rojas, F.J. García-García, S. Järas, M.V. Martínez-Huerta, J.L.G. Fierro, M. Boutonnet, Appl. Catal. A: Gen. 285 (2005) 24.
[28] J. Kaiser, L. Colmenares, Z. Jusys, R. Mörtel, H. Bönnemann, G. Köhl, H. Modrow, J. Hormes, R.J. Behm, Fuel Cells 6 (2006) 190.
[29] Z. Jusys, J. Kaiser, R.J. Behm, Electrochim. Acta 47 (2002) 3693.
[30] G. García, V. Baglio, A. Stassi, E. Pastor, V. Antonucci, A.S. Arico, J. Solid State Electrochem. 11 (2007) 1229.
[31] Z. Liu, J.Y. Lee, M. Han, W. Chen, L.M. Gan, J. Mater. Chem. 12 (2002) 2453.
[32] A.V. Tripkovic, K.D. Popovic, B.N. Grgur, B. Blizanac, P.N. Ross, N.M. Markovic, Electrochem. Acta 47 (2002) 3707.
[33] D. Larcher, R. Patrice, J. Solid State Chem. 154 (2000) 405.
[34] W. Li, C. Liang, W. Zhou, J. Qiu, Z. Zhou, G. Sun, Q. Xin, J. Phys. Chem. B 107 (2003) 6292.
[35] W. Kraus, G. Nolze, J. Appl. Crystallogr. 29 (1996) 301.
[36] H. Yano, M. Kataoka, H. Yamishita, H. Uchida, M. Watanabe, Langmuir 23 (2007) 6438.
[37] J.L. Gómez de la Fuente, S. Rojas, M.V. Martínez-Huerta, P. Terreros, M.A. Peña, J.L.G. Fierro, Carbon 44 (2006) 1919.
[38] C.D. Wagner, W.M. Riggs, L.E. Davis, J.F. Moulder, in: G.E. Muilenberg (Ed.), Handbook of X-Ray Photoelectron Spectroscopy, Perkin-Elmer Corporation, Eden Praire, MN, USA, 1994.
[39] J.L. Gómez de la Fuente, M.V. Martínez-Huerta, S. Rojas, P. Terreros, J.L.G. Fierro, M.A. Peña, Catal. Today 116 (2006) 422.
[40] D. Briggs, M.P. Seah, in: D. Briggs, M.P. Seah (Eds.), Practical Surface Analysis by Auger and X-Ray Photoelectron Spectroscopy, Wiley, New York, 1990.
[41] M.-S. Hyun, S.-K. Kim, B. Lee, D. Peck, Y. Shul, D. Jung, Catal. Today 132 (2008) 138.
[42] T. Yajima, N. Wakabayashi, H. Uchida, M. Watanabe, Chem. Commun. (2003) 828.
[43] A. Kabbabi, R. Faure, R. Durand, B. Bedan, F. Hahn, J.M. Leger, C. Lamy, J. Electroanal. Chem. 444 (1998) 41.
[44] K.J.J. Mayrhofer, B.B. Blizanac, M. Arenz, V.R. Stamenkovic, P.N. Ross, N.M. Markovic, J. Phys. Chem. B 109 (2005) 1443.
[45] U.A. Paulus, A. Wokaun, G.G. Scherer, T.J. Schimdt, V. Stamenkovic, N.M. Markovic, P.N. Ross, Electrochim. Acta 47 (2002) 3787.
[46] S.K. Zecevic, J.S. Wainright, M.H. Litt, S.L. Gojkovic, R.F. Savinell, J. Electrochem. Soc. 144 (1997) 2973.
[47] O. Antoine, Y. Bultel, R. Durand, J. Electroanal. Chem. 499 (2001) 85.
[48] U.A. Paulus, T.J. Schmidt, H.A. Gasteiger, R.J. Behm, J. Eletroanal. Chem. 495 (2001) 134.
[49] S.-B. Han, Y.-J. Song, J.-M. Lee, J.Y. Kim, W. Park, Electrochem. Commun. 10 (2008) 1044.
[50] A.S. Arico, V. Baglio, A. Di Blasi, E. Modica, P.L. Antonucci, V. Antonucci, J. Electroanal. Chem. 557 (2003) 167.
[51] R.K. Raman, A.K. Shukla, A. Gayen, M.S. Hegde, K.R. Priolkar, P.R. Sarode, S. Emura, J. Power Sources 157 (2006) 45.
[52] J.A. Bard, Chem. Rev. 85 (1985) 1.
[53] C. Iwakura, K. Hirao, H. Tamura, Electrochim. Acta 22 (1977) 329.
[54] H.Y.H. Chan, C.G. Takoudis, M.J. Weaver, J. Catal. 172 (1997) 336.